meThe fundamental equation governing the COMPASS force field is provided in (S1), as the following [1]:

$$E=\sum_{b}\left[K_2(b-b_0)^2+K_3(b-b_0)^3+K_4(b-b_0)^4\right] \quad (i)$$

$$+\sum_{\theta}\left[H_2(\theta-\theta_0)^2+H_3(\theta-\theta_0)^3+H_4(\theta-\theta_0)^4\right] \quad (ii)$$

$$+\sum_{\emptyset}\left\{V_1\left[1-cos\left(\emptyset-\emptyset_1{}^0\right)\right]+V_2\left[1-cos\left(\emptyset-2\emptyset_2{}^0\right)\right]+V_3\left[1-cos\left(\emptyset-3\emptyset_3{}^0\right)\right]\right\} \quad (iii)$$

$$+\sum_{x}K_x x^2 \ (iv) +\sum_{b}\sum_{b'}F_{bb'}(b-b_0)\left(b'-b'_0\right) \ (v) +\sum_{\theta}\sum_{\theta'}F_{\theta\theta'}(\theta-\theta_0)\left(\theta'-\theta'_0\right) \ (vi)$$

$$+\sum_{b}\sum_{\theta}F_{b\theta}(b-b_0)(\theta-\theta_0) \ (vii) +\sum_{b}\sum_{\emptyset}(b-b_0)\left[V_1cos\emptyset+V_2cos2\emptyset+V_3cos3\emptyset\right] \ (viii)$$

$$+\sum_{b'}\sum_{\theta}F_{b\theta}\left(b'-b'_0\right)+\left[V_1cos\emptyset+V_2cos2\emptyset+V_3cos3\emptyset\right] \quad (ix)$$

$$+\sum_{\emptyset}\sum_{\theta}\sum_{\theta'}K_{\emptyset\theta\theta'}cos\emptyset(\theta-\theta_0)\left(\theta'-\theta'_0\right) \ (x) +\sum_{i>j}\frac{q_iq_j}{r_{ij}} \ (xi) +\sum_{i>j}\varepsilon_{ij}\left[2\left(\frac{\sigma_{ij}}{r_{ij}}\right)^9-3\left(\frac{\sigma_{ij}}{r_{ij}}\right)^6\right] \ (xii) \quad (S1)$$

In COMPASS, the energy term, E, has been characterized via three major categories, which are namely: (a) the bonded energy (b) the cross-terms and (c) the non-bonded energy contributions. The bonded energy is consisted of contributions (i) – (iv) in (8) such as the following, (i) the covalent bond stretching energy terms (ii) the bond angle bending energy terms (iii) the torsion angle rotation energy terms of the polymeric chains, which has been fitted by a Fourier series function readily available in the software and (iv) the out-of-plane energy or improper term that has been described as a harmonic function. On the other hand, the cross interaction contribution is constituted through the (v) – (x) terms in (8), which encompass the characterization of dynamic variation among bond stretching, bending, and torsion angle rotation. Finally, the last two terms, (xi) and (xii), which are representative terms of the non-bonded energy that illustrate the interactive forces between polymer chains and small molecules, describe the Columbic electrostatic force and van der Waals interaction respectively [2]. Detail description pertaining to the energy contributions can be found elsewhere in published literature [3, 4] and within Materials Studio itself [5].

For the non-bonded Lennard Jones energy term, it has been described with a sixth-order combination rule in order to calculate the corresponding parameters, such as that provided in (S2) and (S3).

$$\sigma_{ij} = \left(\frac{{\sigma_i}^6 + {\sigma_j}^6}{2}\right)^{\frac{1}{6}} \qquad (S2)$$

$$\varepsilon_{ij} = 2\sqrt{\varepsilon_i \varepsilon_j}\left(\frac{{\sigma_i}^3 {\sigma_i}^3}{{\sigma_i}^6 + {\sigma_i}^6}\right) \qquad (S3)$$

In (S2) and (S3), σ_{ij} is the distance at which the potential energy is zero, ε_{ij} corresponds to the well-depth of the interaction potential, while σ_i and ε_i represent the size and energy parameters of the interaction atoms respectively, which are commonly known as the Lennard Jones parameters. As for the Columbic electrostatic term, the partial charges are computed from the charge bond increment, δ_{ij}, which represents charge separation between two valence-bonded atoms [4, 6]. The net charge, q_i, for atom i is a summation of all charge bond increments related to atom i, such as that depicted in (S4).

$$q_i = \sum_j \delta_{ij} \qquad (S4)$$

Supplementary Information

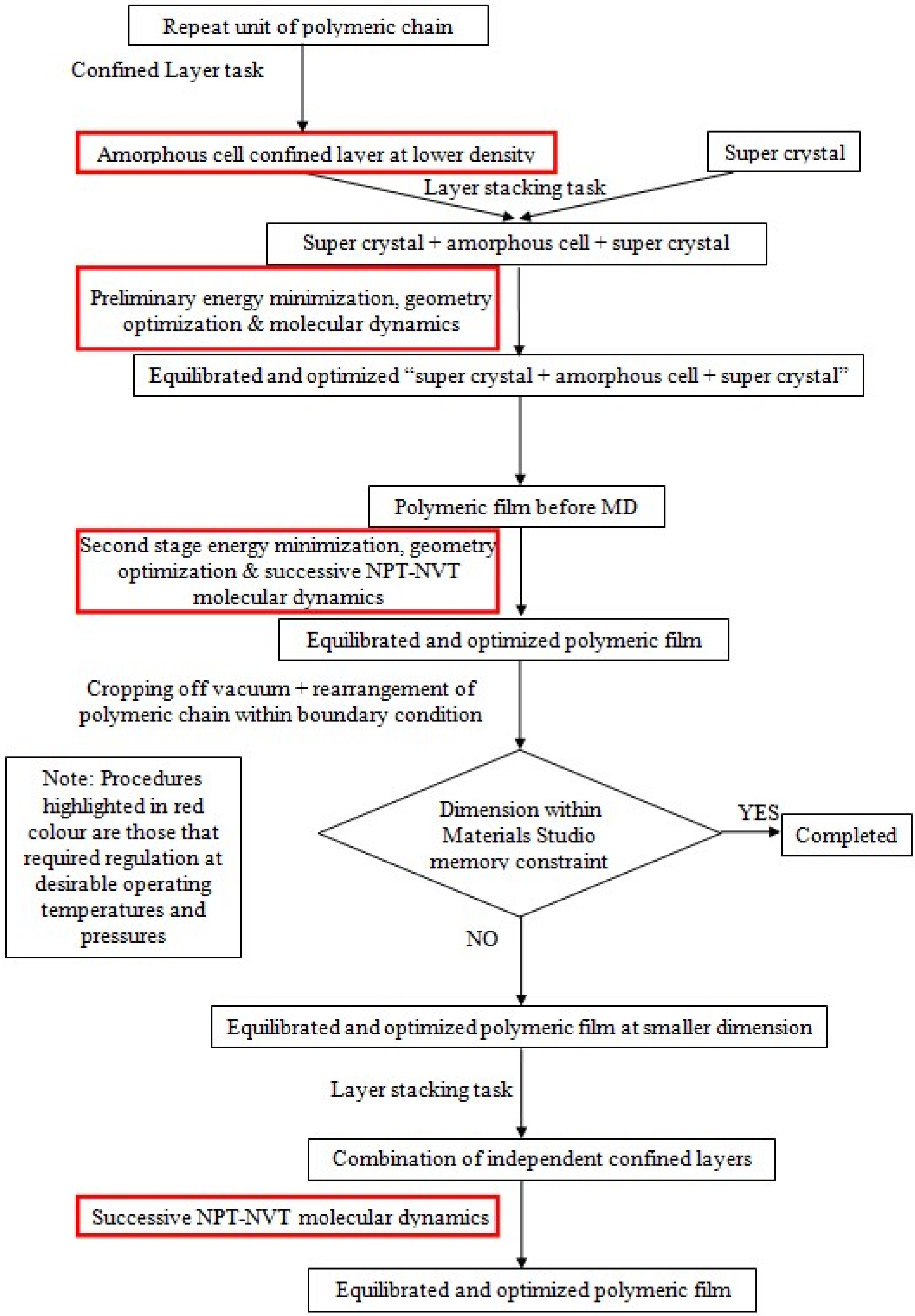

Figure S.1 Overview of Soft Confining Methodology for Ultrathin Films extended to operate at different temperatures and pressures (procedures requiring regulation of temperature and pressure are highlighted in red), adapted from Lock et al. (2017) [7]

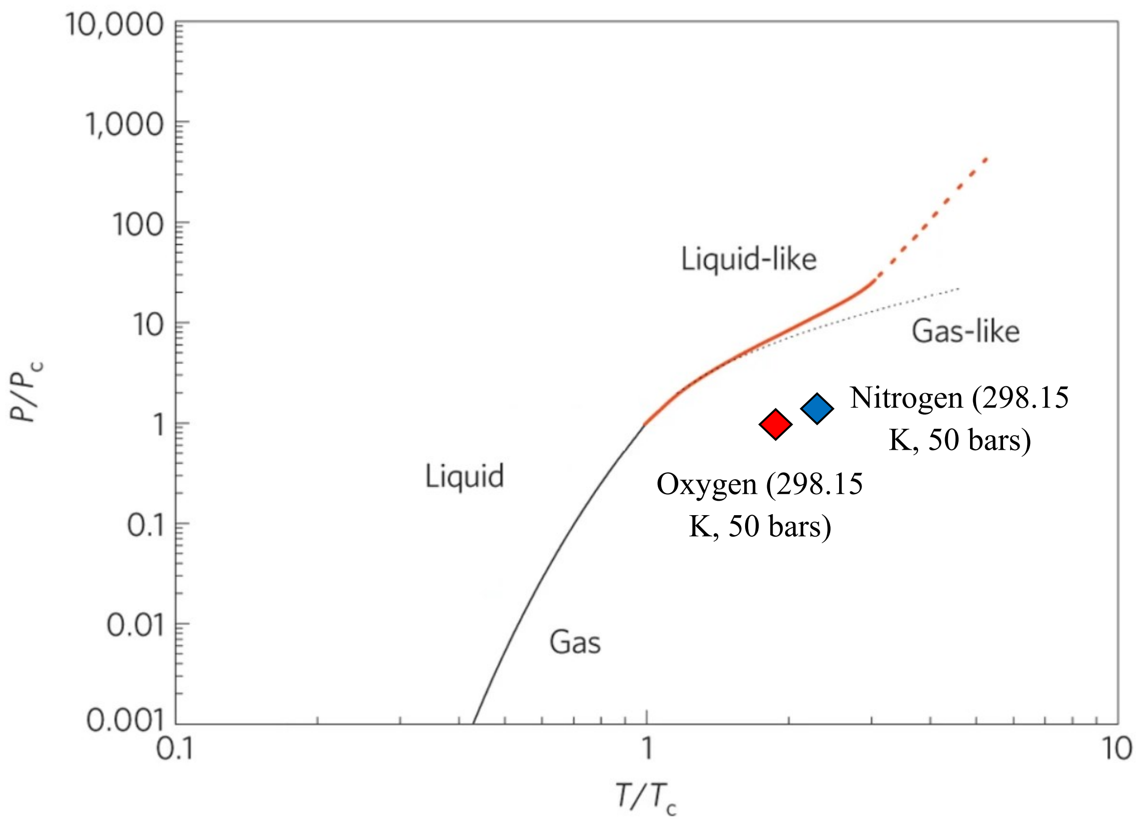

Figure S.2 Schematic representation of gas-liquid existence. Red line: Red line: Widom line of argon obtained from the NIST database (continuous) [8] and its extrapolation (dotted). Black line: best fit of the liquid-vapour coexistence lines for argon, neon, nitrogen and oxygen using the Plank-Riedel equation [9], adapted from Simeoni *et al.* (2010) [10]

(◆ Oxygen and ◆ nitrogen at 298.15 K, 50 bars)

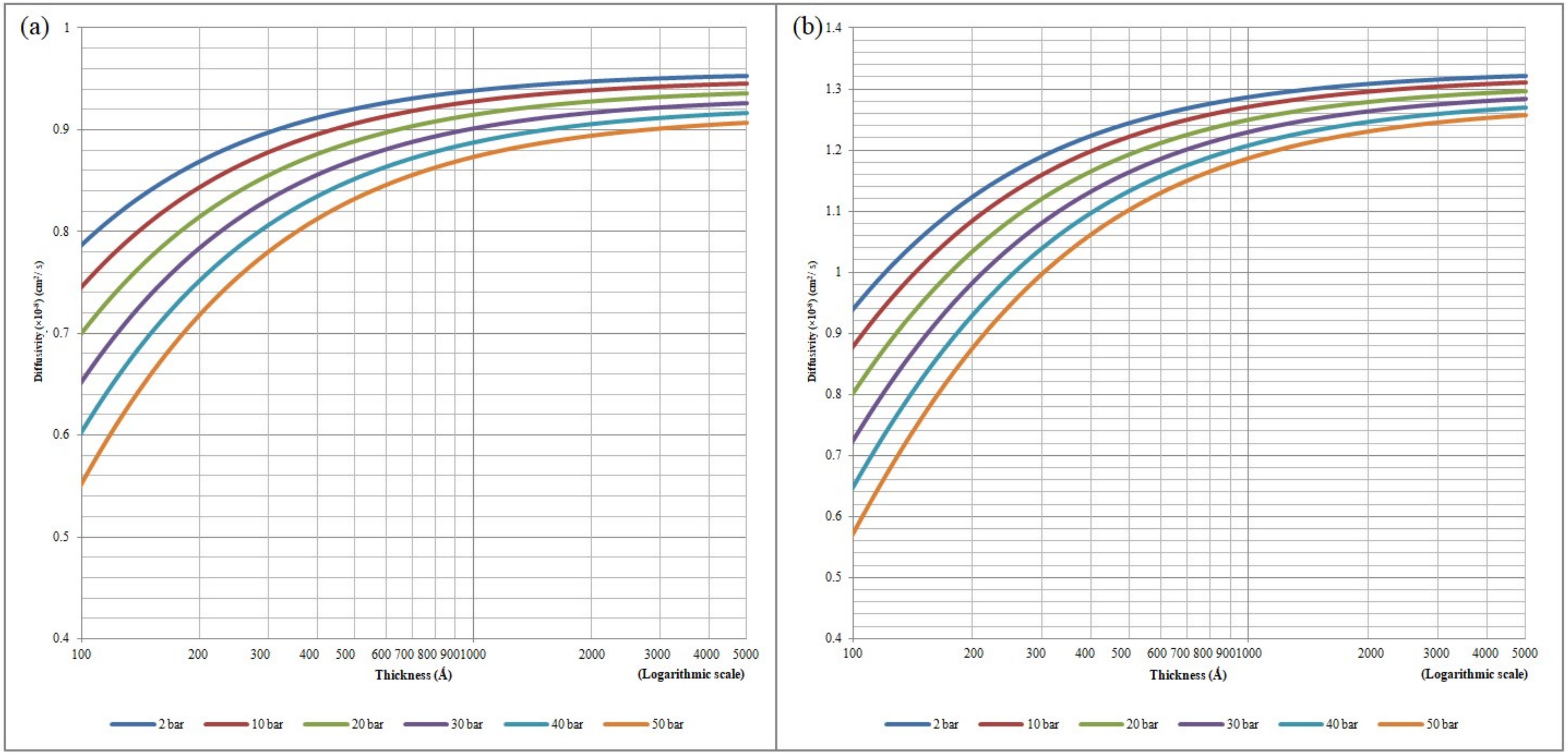

Figure S.3 Effect of thickness upon confinement towards N_2 diffusivity under varying operating pressures of a) 298.15 K b) 308.15 K c) 318.15 K and d) 328.15 K

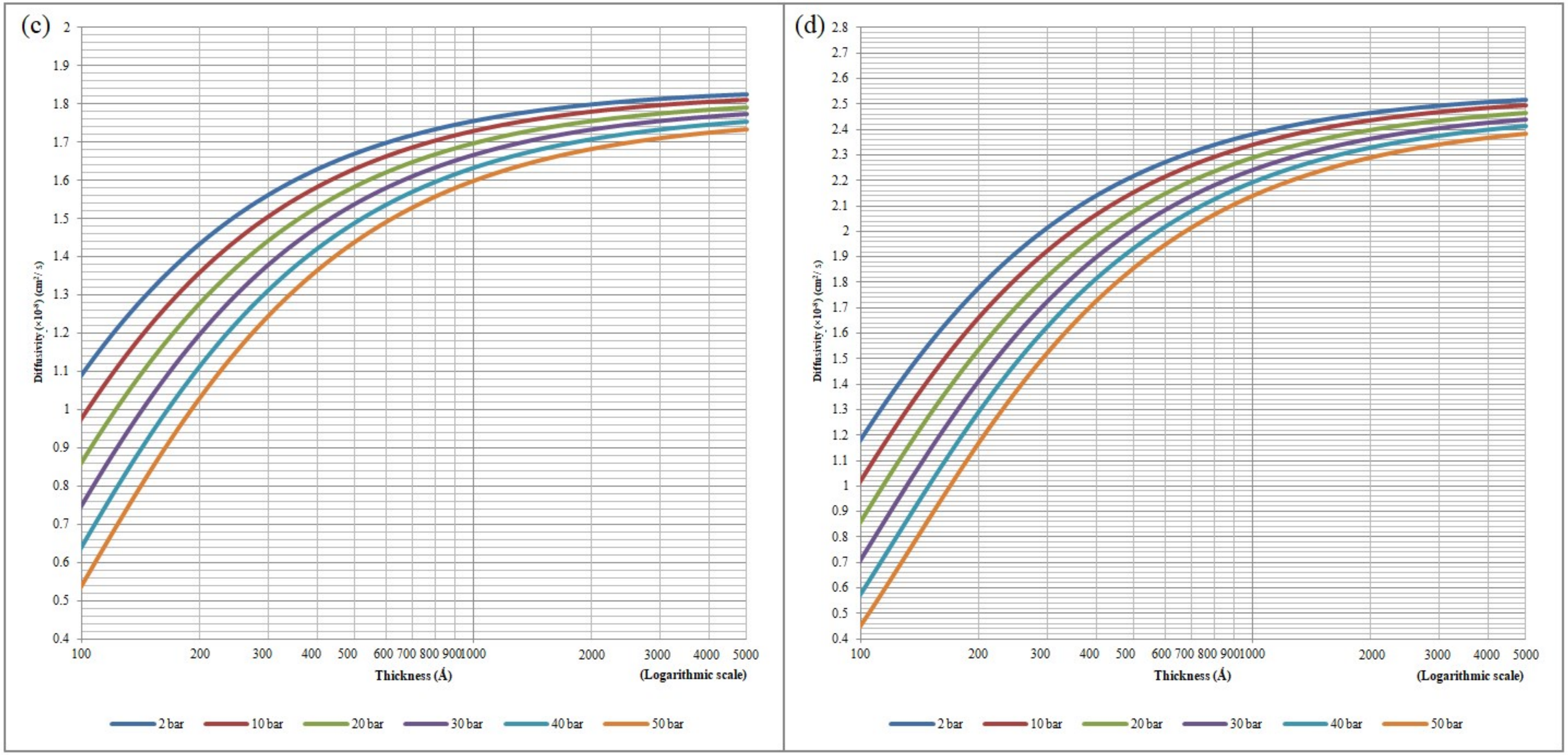

Figure S.3 Effect of thickness upon confinement towards N_2 diffusivity under varying operating pressures of a) 298.15 K b) 308.15 K c) 318.15 K and d) 328.15 K (continued)

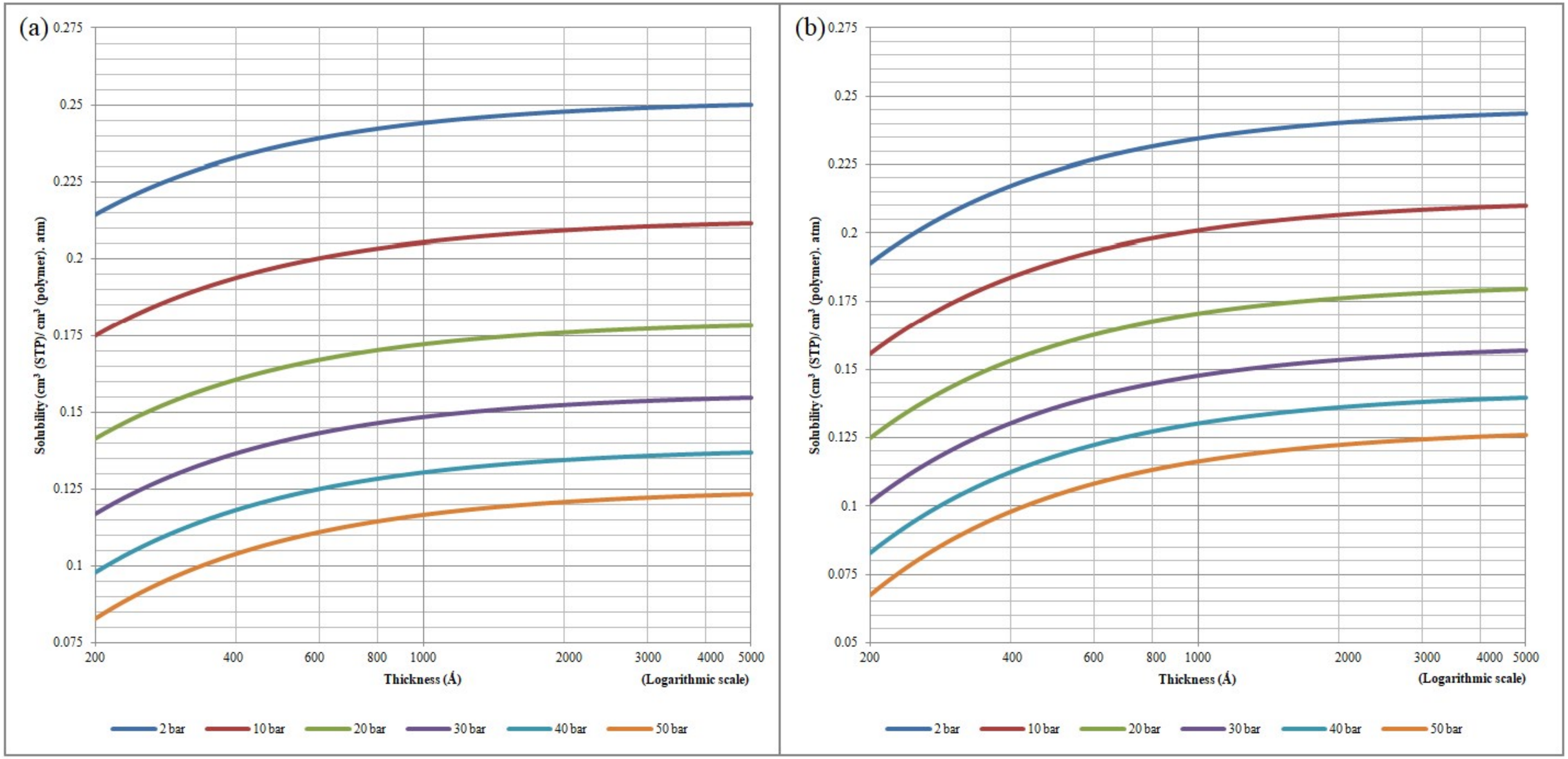

Figure S.4 Effect of thickness upon confinement towards N_2 solubility under varying operating pressures of a) 298.15 K b) 308.15 K c) 318.15 K and d) 328.15 K

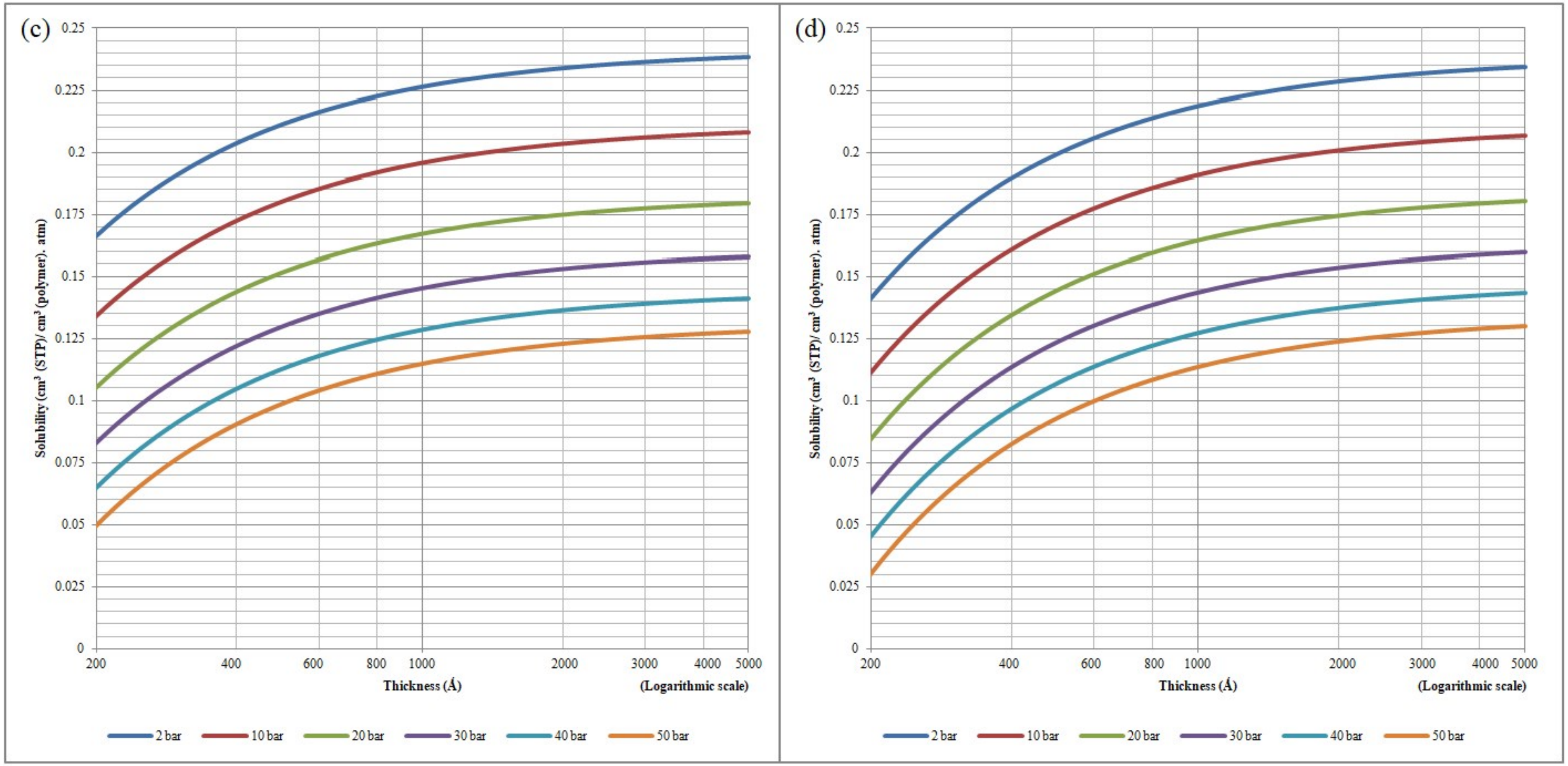

Figure S.4 Effect of thickness upon confinement towards N_2 solubility under varying operating pressures of a) 298.15 K b) 308.15 K c) 318.15 K and d) 328.15 K (continued)

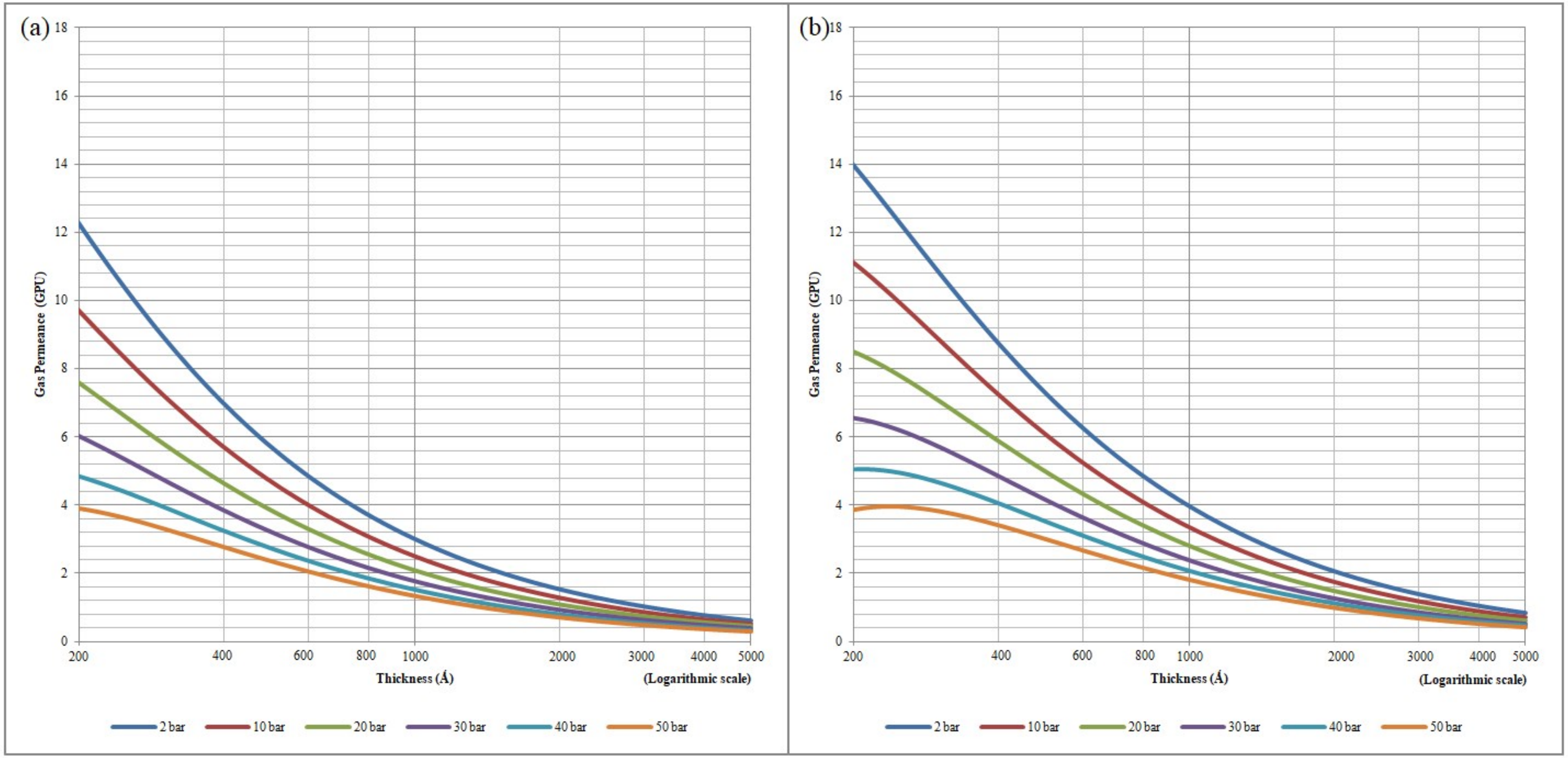

Figure S.5 Effect of thickness upon confinement towards N_2 permeance (pure gas) under varying operating pressures of a) 298.15 K b) 308.15 K c) 318.15 K and d) 328.15 K

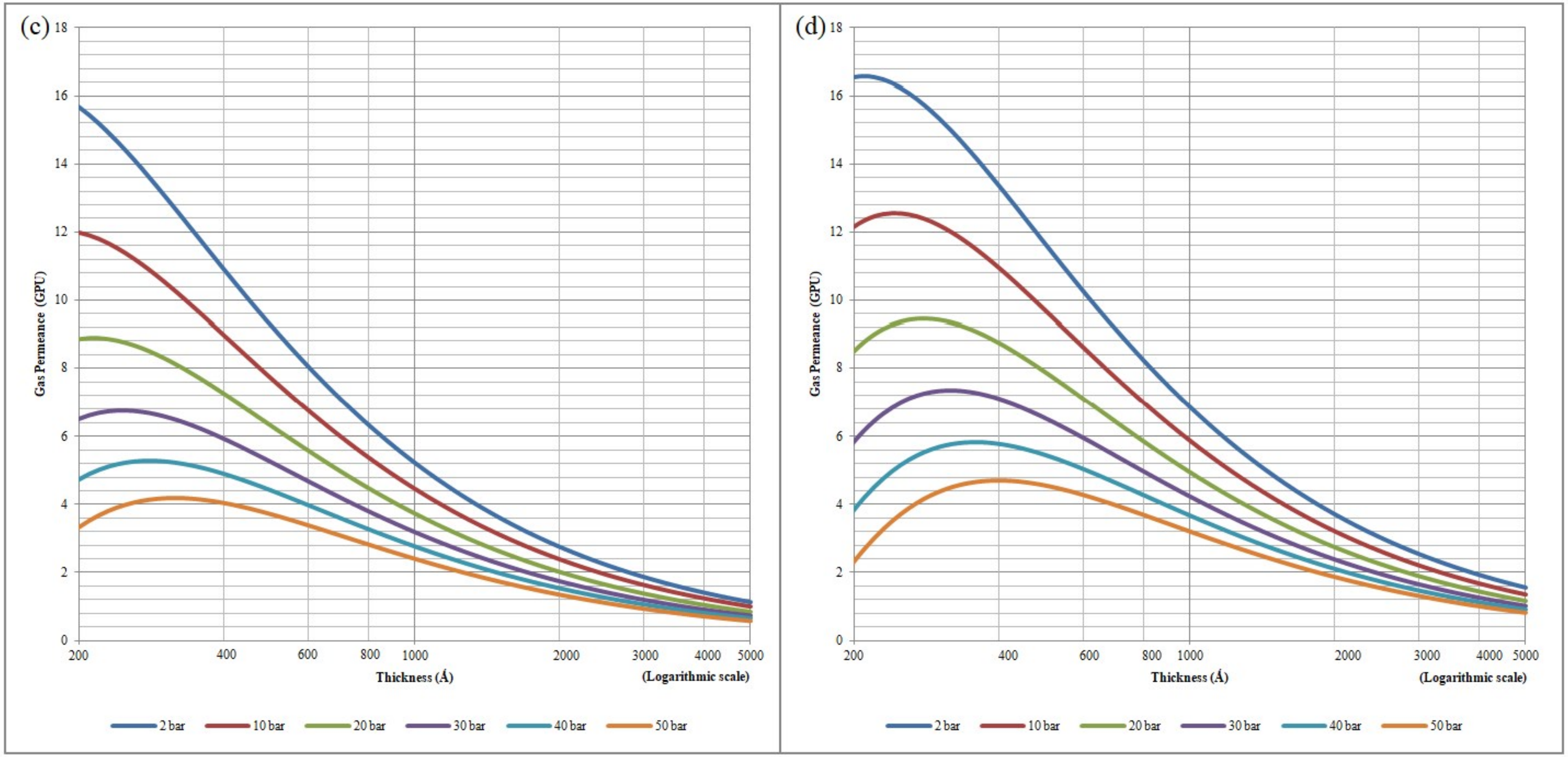

Figure S.5 Effect of thickness upon confinement towards N_2 permeance (pure gas) under varying operating pressures of a) 298.15 K b) 308.15 K c) 318.15 K and d) 328.15 K (continued)

Supplementary Information

Table S.1 Effect of film thickness on the specific volume data of the PSF ultrathin film at different operating temperatures

Thickness (Å) \ Temperature (K)	298.15	303.15	308.15	313.15	318.15	323.15	328.15
~100	0.80333 (±2.53×10^{-4})	0.80297 (±2.62×10^{-4})	0.80273 (±5.33×10^{-4})	0.80112 (±2.74×10^{-4})	0.79992 (±2.82×10^{-4})	0.79873 (±2.18×10^{-4})	0.79655 (±2.30×10^{-4})
~200	0.80497 (±4.90×10^{-4})	0.80508 (±3.16×10^{-4})	0.80514 (±2.74×10^{-4})	0.80515 (±3.01×10^{-4})	0.80522 (±2.16×10^{-4})	0.80548 (±2.71×10^{-4})	0.80572 (±3.00×10^{-4})
~300	0.80599 (±2.92×10^{-4})	0.80618 (±2.40×10^{-4})	0.80623 (±2.22×10^{-4})	0.80722 (±2.39×10^{-4})	0.80743 (±2.94×10^{-4})	0.80777 (±3.44×10^{-4})	0.80806 (±2.95×10^{-4})
~400	0.80615 (±3.27×10^{-4})	0.80696 (±3.03×10^{-4})	0.80721 (±4.25×10^{-4})	0.80801 (±2.86×10^{-4})	0.80874 (±3.35×10^{-4})	0.80884 (±2.49×10^{-4})	0.80925 (±2.14×10^{-4})
~500	0.80674 (±2.94×10^{-4})	0.80714 (±2.87×10^{-4})	0.80727 (±3.48×10^{-4})	0.80819 (±2.96×10^{-4})	0.80892 (±3.09×10^{-4})	0.80933 (±2.72×10^{-4})	0.81006 (±2.89×10^{-4})
~600	0.80690 (±2.31×10^{-4})	0.80726 (±3.20×10^{-4})	0.80760 (±3.23×10^{-4})	0.80852 (±2.22×10^{-4})	0.80945 (±2.72×10^{-4})	0.81006 (±3.11×10^{-4})	0.81038 (±2.57×10^{-4})
~700	0.80698 (±3.13×10^{-4})	0.80735 (±2.35×10^{-4})	0.80803 (±3.15×10^{-4})	0.80878 (±2.41×10^{-4})	0.80953 (±2.57×10^{-4})	0.81014 (±2.56×10^{-4})	0.81046 (±2.68×10^{-4})
~800	0.80714 (±2.64×10^{-4})	0.80751 (±2.33×10^{-4})	0.80842 (±2.14×10^{-4})	0.80918 (±2.75×10^{-4})	0.80993 (±3.14×10^{-4})	0.81046 (±2.75×10^{-4})	0.81070 (±3.09×10^{-4})
~900	0.80731 (±4.32×10^{-4})	0.80775 (±3.24×10^{-4})	0.80886 (±5.80×10^{-4})	0.80941 (±3.53×10^{-4})	0.80997 (±2.93×10^{-4})	0.81049 (±2.20×10^{-4})	0.81095 (±3.40×10^{-4})
~1000	0.80747 (±3.59×10^{-4})	0.80777 (±2.27×10^{-4})	0.80920 (±3.38×10^{-4})	0.80949 (±3.21×10^{-4})	0.81005 (±3.15×10^{-4})	0.81053 (±3.15×10^{-4})	0.81119 (±2.94×10^{-4})

Table S.2 Oxygen diffusivity and solubility data of ~500 Å ultrathin PSF films under varying operating temperature (298.15 to 328.15 K) and pressure (2 to 50 bar)

Temperature (K)	Pressure (bar)	Diffusivity ($\times 10^{-8}$ cm^2/s)	Standard Deviation ($\times 10^{-8}$ cm^2/s)	Solubility (cm^3 (STP)/ cm^3 atm)	Standard Deviation (cm^3 (STP)/ cm^3 atm)
298.15	2	3.2893	±0.0428	0.3702	±0.0052
298.15	10	3.2379	±0.0240	0.3379	±0.0021
298.15	20	3.1887	±0.0410	0.3112	±0.0061
298.15	30	3.1486	±0.0243	0.2901	±0.0047
298.15	40	3.0534	±0.0219	0.2761	±0.0049
298.15	50	2.9912	±0.0362	0.2619	±0.0084
308.15	2	4.1536	±0.0186	0.3254	±0.0056
308.15	10	4.1694	±0.0299	0.3066	±0.0080
308.15	20	4.1411	±0.0160	0.2753	±0.0082
308.15	30	4.0899	±0.0488	0.2598	±0.0075
308.15	40	4.0122	±0.0106	0.2412	±0.0033
308.15	50	3.9533	±0.0366	0.2301	±0.0063
318.15	2	5.4989	±0.0458	0.2912	±0.0067
318.15	10	5.4015	±0.0476	0.2622	±0.0028
318.15	20	5.2087	±0.0159	0.2391	±0.0045
318.15	30	5.1027	±0.0496	0.2188	±0.0037
318.15	40	5.0142	±0.0358	0.1995	±0.0039
318.15	50	4.8763	±0.0435	0.1874	±0.0031
328.15	2	6.9122	±0.0221	0.2576	±0.0048
328.15	10	6.7342	±0.0217	0.2286	±0.0032
328.15	20	6.7089	±0.0140	0.2051	±0.0046
328.15	30	6.4672	±0.0351	0.1827	±0.0068
328.15	40	6.2129	±0.0352	0.1681	±0.0030
328.15	50	6.1173	±0.0233	0.1557	0.0053

Table S.3 Nitrogen diffusivity and solubility of ~500 Å ultrathin PSF films under varying operating temperature (298.15 to 328.15 K) and pressure (2 to 50 bar)

Temperature (K)	Pressure (bar)	Diffusivity ($\times 10^{-8}$ cm^2/s)	Standard Deviation ($\times 10^{-8}$ cm^2/s)	Solubility (cm^3 (STP)/ cm^3 atm)	Standard Deviation (cm^3 (STP)/ cm^3 atm)
298.15	2	0.9227	±0.0134	0.2381	±0.0051
298.15	10	0.9078	±0.0166	0.1994	±0.0046
298.15	20	0.8743	±0.0301	0.1652	±0.0032
298.15	30	0.8655	±0.0386	0.1394	±0.0026
298.15	40	0.8337	±0.0398	0.1229	±0.0084
298.15	50	0.8215	±0.0142	0.1092	±0.0032
308.15	2	1.1362	±0.0233	0.2215	±0.0079
308.15	10	1.1204	±0.0385	0.1924	±0.0076
308.15	20	1.1189	±0.0342	0.1601	±0.0024
308.15	30	1.1162	±0.0460	0.1378	±0.0030
308.15	40	1.1106	±0.0361	0.1201	±0.0032
308.15	50	1.0824	±0.0122	0.1043	±0.0065
318.15	2	1.6881	±0.0115	0.2132	±0.0026
318.15	10	1.6691	±0.0247	0.1810	±0.0064
318.15	20	1.5923	±0.0405	0.1538	±0.0066
318.15	30	1.5528	±0.0435	0.1295	±0.0068
318.15	40	1.5011	±0.0257	0.1137	±0.0036
318.15	50	1.4231	±0.0311	0.1005	±0.0039
328.15	2	2.2312	±0.0303	0.2001	±0.0058
328.15	10	2.1672	±0.0191	0.1739	±0.0057
328.15	20	2.0823	±0.0351	0.1458	±0.0079
328.15	30	2.0341	±0.0434	0.1249	±0.0050
328.15	40	1.9568	±0.0453	0.1078	±0.0028
328.15	50	1.8912	±0.0355	0.0953	±0.0023

References

1. K. Golzar, S. Amjad-Iranagh, M. Amani and H. Modarress, *J. Membr. Sci.*, 2014, **451**, 117–134.
2. K.-S. Chang, Y.-H. Huang, K.-R. Lee and K.-L. Tung, *J. Membr. Sci.*, 2010, **354**, 93-100.
3. H. Sun, P. Ren and J. R. Fried, *Comput. Theor. Polym. Sci.*, 1998, **8**, 229-246.
4. H. Sun, *J. Phys. Chem. B*, 1998, **102**, 7338-7364.
5. *Journal*, 2015.
6. J. Yang, Y. Ren, A.-M. Tian and H. Sun, *J. Phys. Chem. B*, 2000, **104**, 4951-4957.
7. S. S. M. Lock, K. K. Lau, A. M. Shariff, Y. F. Yeong and A. M. Bustam, *RSC Adv.*, 2017, **7**, 44376-44393.
8. NIST Chemistry WebBook, http://webbook.nist.gov/chemistry/.
9. F. Gorelli, M. Santoro, T. Scopigno, M. Krisch and G. Ruocco, *Phys. Rev. Lett.*, 2006, **97**, 245702.
10. G. G. Simeoni, T. Bryk, F. A. Gorelli, M. Krisch, G. Ruocco, M. Santoro and T. Scopigno, *Nat. Phys.*, 2010, **6**, 503-507.